Analysis on Bouguer Gravity Anomaly Characteristics and Boundary Identification in China and Surrounding Regions

Zhixin Xue

Institute of Geodesy and Geophysics Chinese Academy of Sciences https://orcid.org/0000-0001-8660-8823

Dongmei Guo (guodongmei@whigg.ac.cn)

University of the Chinese Academy of Sciences

Panpan Zhang

Chinese Academy of Sciences Innovation Academy for Precision Measurement Science and Technology

Full paper

Keywords: Bouguer gravity anomaly, Gravity interpretation, Tectonic stress field, Edge detection, Tectonic division

Posted Date: October 29th, 2020

DOI: https://doi.org/10.21203/rs.3.rs-96900/v1

Version of Record: A version of this preprint was published at Terrestrial, Atmospheric and Oceanic Sciences on January 1st, 2021. See the published version at https://doi.org/10.3319/TAO.2021.06.22.02.

Analysis on Bouguer Gravity Anomaly Characteristics and Boundary Identification in China and Surrounding Regions

Zhixin Xue[1,2], Dongmei Guo[1,2], Panpan Zhang[1,2]

Zhixin Xue: xuezhixin@asch.whigg.ac.cn

Dongmei Guo: guodongmei@whigg.ac.cn

Panpan Zhang: zhangpanpan@asch.whigg.ac.cn

Abstract: China is located in the southeast of the Eurasian Plate and is subject to the effects of subducting, squeezing and collision by the Pacific Plate to the east, Philippine Plate to the southeast and Indian Ocean Plate to the southwest. It has exceptional geotectonic structure. Based on the satellite gravity data with high precision, high resolution and ample geophysical information, combined with geological data, by using satellite gravity potential field and its full tensor gradient, this paper studies the distribution characteristics of gravity anomalies and the identification of tectonic boundaries in China and surrounding regions. Results suggest that the Bouguer gravity anomaly in eastern China reduces gradually from east to west, mostly in the direction of NNE; in the western, it reduces gradually in a wave mode from north to south, mainly in the directions of NW and NWW. In general, the stress field reduces gradually from west to east, and the tectonic of stress field in western China is complex. The maximum principal compressive stress in Xinjiang exists in SN direction and that in Qinghai-Tibet Plateau mostly changes gradually from NNE to SSE; the change in eastern China is relatively simple, and the maximum principal compressive stress direction gradually changes from NE to WE and then to SE. In addition to the above study results, by comprehensively referencing the previous studies by other people and by using the boundary identification methods based on the satellite gravity full-tensor gradient data and its combinations, we update the extension route of Red River fault zone and deduce the tectonic unit boundary between the North China and South China active tectonic block regions. This paper identifies in China and surrounding regions 6 primary active tectonic blocks, 22 secondary active tectonic blocks, 3 tertiary active tectonic blocks and the 20 active tectonic block boundary zones constituted of deformation belts and active tectonic belts with various geometric structures and width variations. The results of this study can improve the understanding of gravity anomalies and boundary structures in China and surrounding regions, and provide certain geophysical supports for geological structure analysis and crustal dynamic process.

Keywords: Bouguer gravity anomaly; Gravity interpretation; Tectonic stress field; Edge detection; Tectonic division

0 Introduction

China is located in the southeast of the Eurasian Plate and is subject to the effects of subducting, squeezing and collision by the Pacific Plate to the east, Philippine Plate to the southeast and Indian Ocean Plate to the southwest. With its exceptional geotectonic structure, this

Correspondence: guodongmei@whigg.ac.cn

[1] State Key Laboratory of Geodesy and Earth's Dynamics, Innovation Academy for Precision Measurement Science and Technology, Chinese Academy of Sciences, Wuhan 430077, China

[2] University of the Chinese Academy of Sciences, Beijing 100049, China

country has always drawn high attention from domestic and foreign scholars. After the plate tectonics theory was introduced to China in late 20th century, numerous renowned scholars have offered innovative insights regarding the geotectonic structure of China (Li 1973; Huang et al. 1980; Li et al. 1982; Zhang 1986; Ren 1999; Deng et al. 2002; Zhang et al. 2003; Zhang et al. 2005). In the last century, many scholars have tried many methods from many aspects to add to and update the understanding of China's geological structure (Pan et al. 2009, 2015; Xiong et al. 2015a, b, c, 2018), which has been crucial to the study on geotectonic zoning and evolution of China and prediction and prospecting of mineral resources.

Gravity anomalies indicate uneven density underground, which has been extensively used for resources prospecting, endogenous dynamics study and geological structure analysis. Gravity anomaly is uniquely advantageous in stress field calculation and boundary identification. Wei et al. (1981) used the gravity data measured on ground surface to calculate and thereby plot the free-air gravity anomaly map of China. On this basis, they discussed over the tectonic, isostasy principle, seismic activities and possible geodynamic processes. Ma et al. (2006) analyzed and compared the colored graphics of Bouguer gravity anomaly horizontal gradient of China mainland and discussed over the new tentonic characteristics of China and surrounding regions. Yang et al. (2016) used the new information extraction methods, such as wavelet multi-scale, made correlations in the earth gravity field model (EGM2008) to obtain the satellite Bouguer gravity anomaly data of China and surrounding areas, so as to extract and invert the density information of the upper, middle and lower parts of the crust in China and surrounding areas, which revealed the three-dimensional density structure of the regions. Lu et al. (2020) used the topography and Bouguer gravity anomaly data to make detailed analysis on effective elastic thickness of China and surrounding

regions. You (1994) was the first person to use gravity data to measure the horizontal tectonic stress field. Xie et al. (2004) proposed the principles for tectonic stress zoning of China and surrounding regions, completed classification of tectonic stress field and further analyzed the relevant dynamic environment. Xu et al. (2008) used the focal mechanism solutions of strong earthquakes to investigate how the stress field structure of China mainland and surrounding plates will impact the stress field of China mainland.

The gravity anomaly data include ample geophysical information, which can be analyzed and interpreted in greater detail by using effective information processing methods. Gravity full-tensor gradient data, which has greater resolution than gravity anomaly, can be used to obtain higher derivatives, isolate superimposed anomaly information and further interpret geological characteristics. Gravity full-tensor gradient and its combinations have been extensively used for boundary identification. Miller et al. (1994) proposed the concept of "tilt angle", i.e. the ratio between potential field vertical derivative and absolute value of horizontal derivative, where the zero isoline is used to identify the boundaries of the anomalous underground geological bodies at different depths. Verduzco et al. (2004) used the total horizontal derivative of tilt angle to detect the boundaries of geological bodies. Nabighian (1984) and Roest et al. (1992) discovered that the maximum amplitude of analytic signal can directly describe density and the boundary of magnetic body. Total horizontal derivative (Cordell 1979; Cordell et al. 1985) has greater resolution in boundary identification effect than analytic signal. Theta map (Wijns et al. 2005) is based on analytic signal and can identify anomaly signals of minor amplitude.

This paper uses the satellite gravity potential field and full-tensor gradient data in the V27.1 Gravity Model published by SIO (Scripps Institution of Oceanography) to investigate the gravity

anomalies distribution in China and surrounding regions and to identify the tectonic boundaries. First, we use free-air gravity anomaly and topography data to calculate the terrestrial-marine Bouguer gravity anomaly of East Asia and analyze the characteristics of the resources and structures inside the crust that deviate from normal density distribution; Then we use the Bouguer gravity anomaly to identify the tectonic stress field and discuss the distribution characteristics of the tectonic movements of China and surrounding regions and their dynamics; Finally, we use satellite gravity full-tensor gradient data and its combinations to identify the tectonic boundaries of faults, contact zones and other tectonic units and thereby divide the geological tectonic units of East Asia, identify the general outlines of the microplates and provide the tectonic basis for geological interpretation.

1 Theory

1.1 Tectonic Stress Field

Tectonic stress field, that is, at a certain moment, there is a stress field inside the crust within a certain range that causes structural deformation and fracture. There is a close relationship between gravity field the tectonic stress field. According to the Bouguer gravity anomaly, the Hilbert three-dimensional space potential field conversion formula can be used to derive the sum of the horizontal components of gravity at a certain point (x,y) (You 1994) , as shown in the following formula

$$\begin{cases} g_x = -\dfrac{1}{2\pi}\displaystyle\int_{-\infty}^{+\infty}\int_{-\infty}^{+\infty}\dfrac{(\mathrm{x}-\xi)g_z}{[(x-\xi)^2+(y-\eta)^2+H^2]^{3/2}}\mathrm{d}\xi\mathrm{d}\eta \\ g_y = -\dfrac{1}{2\pi}\displaystyle\int_{-\infty}^{+\infty}\int_{-\infty}^{+\infty}\dfrac{(y-\eta)g_z}{[(x-\xi)^2+(y-\eta)^2+H^2]^{3/2}}\mathrm{d}\xi\mathrm{d}\eta \end{cases} \quad (1)$$

Where (ζ,η) is the flow coordinates throughout the whole measurement area, g_z is the

97 corresponding Bouguer gravity anomaly value; H is the spatial continuation height; the integration
98 area in the above formula can be finite and grid discretized.

99 The maximum principal compressive stress direction A of the stress field can be determined
100 by the horizontal direction of gravity, as shown in the following formula

101 $$\beta = \arctan \frac{g_y}{g_x} \tag{2}$$

102 The formula for calculating the tectonic stress field from gravity anomaly is shown below
103 (Guo et al. 2017)

104 $$\Delta\sigma_{xx} = \frac{g\rho_i g_h}{4\pi f \rho_m} \tag{3}$$

105 where ρ_i is the density of the unit plot, ρ_m is the density of the mantle, which are respectively taken
106 as 2670 kg/m^3 and 3300 kg/m^3; g is the average acceleration of gravity, f is the gravitational
107 constant, $\Delta\sigma_{xx}$ is the horizontal component of gravity, and g_h is the horizontal component of
108 gravity , namely $g_h = (g_x^2 + g_y^2)^{1/2}$.

109 1.2 Boundary Identification Methods

110 The gravity potential has continuous partial derivatives of various orders, but many
111 higher-order derivatives cannot be derived directly from the gravity potential. Through Fourier
112 transform, the full tensor gradient of gravity can be calculated from the vertical gravity anomaly
113 (Mickus et al. 2001).

114 $$\Gamma = F^{-1} \quad K(k)\ V_z(k) \tag{4}$$

115 in the above formula, F^{-1} is the two-dimensional inverse Fourier transform, $V_z(k)$ is the
116 two-dimensional Fourier transform of vertical gravity anomaly; K is the wave number vector,
117 $|k| = (k_x^2 + k_y^2)^{1/2}$, and $|k| \neq 0$. The $K(k)$ expression is as follows

$$K(k)=\begin{bmatrix} \frac{-k_x^2}{|k|} & \frac{-k_x k_y}{|k|} & -ik_x \\ \frac{-k_x k_y}{|k|} & \frac{-k_y^2}{|k|} & -ik_y \\ -ik_x & -ik_y & |k| \end{bmatrix} \tag{5}$$

where k_x and k_y are the wave numbers in the x and y directions respectively, and i is the imaginary unit.

The gravity gradient tensor is the second derivative of the gravity potential. According to the above formula, the expression of the gravity gradient tensor Γ is as follows

$$\Gamma_{i,j}=\begin{bmatrix} V_{xx} & V_{xy} & V_{xz} \\ V_{yx} & V_{yy} & V_{yz} \\ V_{zx} & V_{zy} & V_{zz} \end{bmatrix} \tag{6}$$

where $i = x, y, z, j = x, y, z$.

It can be seen from the above formula that the nine gravity gradient tensors are symmetric: $V_{ij} = V_{ji}$, of which five components are independent of each other, and the remaining four components can be derived accordingly. V is the gravitational potential, and its components V_{xx}, V_{yy}, and V_{zz} satisfy the Laplace equation, namely $V_{xx}^2 + V_{yy}^2 + V_{zz}^2 = 0$.

On the basis of the above calculations, this paper uses boundary detectors composed of gravity full tensor gradients and its different combinations for boundary identification. The detailed combinations are shown below.

The total horizontal derivative THD can be described by

$$\mathrm{THD} = \sqrt{V_{xz}^2 + V_{yz}^2} \tag{7}$$

The analytic signal ASM can be described by

$$\mathrm{ASM} = \sqrt{V_{xz}^2 + V_{yz}^2 + V_{zz}^2} \tag{8}$$

The tilt derivative TDR can be described by

$$\mathrm{TDR} = \arctan\left(\frac{V_{zz}}{\sqrt{V_{xz}^{\ 2} + V_{yz}^{\ 2}}}\right) \tag{9}$$

The total horizontal derivative of the tilt derivative THDR can be described by

$$\mathrm{THDR} = \sqrt{\left(\frac{d\mathrm{TDR}}{dx}\right)^2 + \left(\frac{d\mathrm{TDR}}{dy}\right)^2} \tag{10}$$

The Theta map θ can be described by

$$\theta = \arccos\left(\frac{\sqrt{V_{xz}^{\ 2} + V_{yz}^{\ 2}}}{\sqrt{V_{xz}^{\ 2} + V_{yz}^{\ 2} + V_{zz}^{\ 2}}}\right) \tag{11}$$

2 Data

The study scope of this paper is 65° E-145° E, 0° N-60° N; the gravity and topography data are sourced from the V27.1 Gravity Model published by Scripps Institution of Oceanography (SIO) in 2018 and the V18.1 Topography Model in 2014, where the spatial resolution of the data is 1′×1′. The SIO V27.1 Gravity Model consists of the land gravity anomaly data of EGM2008 (Earth Gravitational Model, 2008) and ocean gravity anomaly data from satellite altimetry.

2.1 Topography data

This paper uses the V18.1 Topography Model published by SIO in 2014, with spatial resolution 1′×1′ ; the data cover 0° E-360° E longitude and -80.738° N-80.738° N latitude; the vertical datum is the sea level; elevation is in m; Mercator projection is used. Fig. 1 shows the topographic map of China and surrounding regions.

As shown in Fig. 1, China has numerous mountains and complex and diverse terrains; it has three steps of topography, with the west parts higher than the east parts; the mountains constitute a network that exists throughout China mainland. The first step has average altitude of above 4500 m and contains the Qinghai-Tibet Plateau of Southwest China and the Qaidam Basin. To the east

and north of the second step are Kunlun Mountains-Altyn Tagh Mountains-Qilian Mountains-Hengduan Mountains, which is the boundary between the first and second steps; to the east are the Great Higgnan Mountains-Taihang Mountains-Wushan Mountain-Xuefeng Mountain, which is the boundary between the second step and third step. The second step has average altitude of 1000-2000 m and contains large basins and plateaus, e.g. Tarim Basin and Sichuan Basin. The third step, located to the east of the second step, has altitude of mostly less than 500 m and flat terrain, e.g. North China Plain. To the east of the third step is the continental shelf, which is the extension of China Mainland into the ocean. Overall, Fig. 1 accurately indicates China's topographic characteristics, where the west is higher than the east and south higher than the north. The maximum topography elevation exists in the Hengduan Mountains and Tianshan Mountains, from which the elevation reduces in both directions; the minimum elevation exists in the flat areas in East China.

Fig.1 The topographic map in China and surrounding regions
Black solid line represents the national boundary of China. HDM (Hengduan Mountains), GHM (Great Higgnan Mountains), CBM (Changbai Mountains), THM (Taihang Mountains), HLM (Helan Mountains), LPM (Liupan Mountains), LMM (Longmenshan Mountains), WS (Wu Shan), WMM (Wumeng Mountains), WLM (Wuling Mountains), XFM (Xuefeng Mountains). The symbols in the following figures have the same meaning.

2.2 Free-air gravity anomaly

Free-air gravity anomaly changes drastically in the areas with great terrain undulation. As shown in Fig. 2, the areas with great terrain undulation have clearly identifiable boundaries between mountains and basins, which is highly indicative of the structure of the tectonic blocks in the study area. The east and west parts of China, with largely 105° E between them, have

significant difference in free-air gravity anomaly. East China has generally flat terrain and therefore mild anomaly variation; West China has great terrain undulation and therefore drastic anomaly variation.

East China has two noticeable NNE positive linear anomaly belts. One starts from Changbai Mountain in Northeast China, extends along Shandong Peninsula and towards the coastal areas of Zhejiang and Fujian; the other one starts from Great Higgnan Mountains, extends along Taihang Mountains, passes the Yinshan Mountains and Qinling Mountains which are nearly in EW direction and extends towards to West Hubei and West Hunan. Due to the Ordos Basin and Sichuan Basin, the NNE linear anomaly is not continuous and has distortion along the way. The plain area between the two anomaly belts has mild anomaly amplitude variation, occasionally negative but mostly positive.

West China has drastic anomaly variation, with positive and negative anomalies alternating with each other. The drastic variation of anomaly amplitude perfectly corresponds to the topographic characteristics shown in Fig. 1. Tarim Basin, Qaidam Basin and Junggar Basin mostly have negative anomalies. The Qinghai-Tibet Plateau has clearly identifiable boundary, where the surrounding mountains all have positive anomalies and drastic variation and the Himalayas have immense anomaly variation amplitude. The west of Qinghai-Tibet Plateau also has noticeably drastic positive anomaly variation, but positive anomalies and negative anomalies alternate with each other in the interior of Qinghai-Tibet Plateau, with mild anomaly variation.

Fig.2 The Free Air gravity anomaly in China and surrounding regions

JN is Jinan, the capital of Shandong Province; WH is Wuhan, the capital of Hubei Province; CS is Changsha, the capital of Hunan Province; HZ is Hangzhou, the capital of Zhejiang Province; FZ is the capital of Fujian Province. The symbols in the following figures have the same meaning.

3 Analysis on Bouguer Gravity Anomaly Characteristics and Tectonic Characteristics

3.1 Bouguer gravity anomaly

By using the free-air gravity anomaly data and topography data obtained and making Bouguer correction and terrain correction (Fullea et al. 2008), the 1′×1′ complete Bouguer gravity anomaly is obtained (Fig. 3). In Bouguer gravity anomaly correction, all masses outside the geoidal surface are removed and some of the masses are filled into the oceans. Therefore it can be believed that Bouguer gravity anomaly includes the impacts of the resources and structures inside the crust that deviate from the normal density distribution and also the horizontal impacts of undulation of the lower crustal interface relative to the mass of lower mantle.

As indicated in Fig. 3, among the Bouguer gravity anomalies, the east ones are higher than the west ones and north ones higher than south ones. The Bouguer gravity anomaly, approx. -740 mGal, exists in Qinghai-Tibet Plateau; the value increases gradually eastward and northward; the eastern coastal region of China has low Bouguer gravity anomaly. The east and west parts of China, with largely 105° E between them, have significant difference in Bouguer gravity anomaly. The eastern region has mild Bouguer gravity anomaly variation, while the western region has drastic Bouguer gravity anomaly variation.

In East China, Bouguer gravity anomaly reduces gradually from east to west, largely in the NNE direction, e.g. the two Bouguer gravity anomaly gradient belts that run from north to south of China. One is the gravity gradient belt through Great Higgnan Mountains-Taihang Mountains-Wuling Mountain, which has relatively dense Bouguer gravity anomaly isoline. The other one is the gravity anomaly gradient belt through Helan Mountain-Liupan

Mountain-Longmenshan Mountains-Wumeng Mountain. The east and west parts of this gradient belt differ immensely in Bouguer gravity anomaly. In the eastern coastal areas in Zhejiang and Fujian, there is a smaller gravity anomaly gradient belt, in which gravity anomaly is mostly negative. To its north, gravity anomaly has mild variation and is mostly positive. Near the Great Higgnan Mountains-Taihang Mountains-Wuling Mountain gravity anomaly gradient belt, gravity anomaly has drastic variation and becomes negative.

In West China, the minimum gravity anomaly is approx. -80 mGal in Junggar region in the north and approx. -740 mGal in Qinghai-Tibet Plateau; Bouguer gravity anomaly generally reduces in a wave mode from north to south; largely in the NW and NWW directions, there are four obvious gravity gradient belts. One is the gravity gradient belt through the Altai Mountains and Tianshan Mountains in the north; one is the gravity gradient belt through the Altyn Tagh Mountains and Qilian Mountains, which bends from west to south; one is the gravity gradient belt through the Qimantag Mountains and Burhan Budai Mountains in the south of Qaidam Basin, which bends from west to southeast; one is the gravity gradient belt through the Himalaya Mountains and Hengduan Mountains, which extends in arc-like form. Gravity anomaly has drastic variation along the margin of plateau and mild variation within plateau.

Fig.3 The Bouguer gravity anomaly in China and surrounding regions

3.2 Tectonic stress field analysis

The driving force for geologic structure is lateral pressure, which causes stress field changes inside the crust. On this basis, tectonic stress can be used to analyze the dynamic characteristics of crustal movement. By using the three-dimensional space potential field conversion formula of

249 Hilbert (You 1994), the tectonic stress field of China and surrounding regions is calculated (Guo et
250 al. 2017), as shown in Fig. 4.

251 China and surrounding regions are located in the southeast of Eurasian Plate and are subject
252 to the effects of subducting, squeezing and collision by the Pacific Plate to the southeast,
253 Philippine Plate to the southeast and Indian Ocean Plate to the southwest. The strong effects of the
254 surrounding plates have given rise to the unique lithospheric stress field and tectonic movement.
255 Collision with the Indian Ocean Plate has significantly changed the geological structure of
256 Western China and is the main factor that has generated the exceptional tectonic stress field of
257 China mainland. The tectonic stress in China and surrounding regions is noticeably zoned and
258 non-uniform and generally reduces gradually from west to east. The stress is greater in West China
259 than in East China.

260 In East China, China mainland and surrounding areas are subject to the squeezing action in
261 NEE-SWW direction, which is basically the direction in which the Pacific Plate and Philippine
262 Plate jointly impose subduction to the Eurasian Continent. In the GPS horizontal velocity field in
263 Fig. 5 (Zhao et al. 2015), the Pacific Plate and Philippine Plate have great velocity in the NW
264 direction. The maximum principal compressive stress resulting from the subduction jointly
265 imposed by the surrounding plates is in NE-NEE direction in Northwest China and North China
266 and in NW-SE direction in South China. As shown in Fig. 5, the North China and South China
267 tectonic blocks generally move to the southeast and faster the further south; the areas near the
268 northeast tectonic block are the slowest.

269 In West China, China mainland and surrounding regions are subject to squeezing in largely
270 the SN-NNE direction, which is basically the direction in which the Indian Ocean Plate impose the

northward collision to the Eurasian Continent. As shown in Fig. 5, the Indian Plate moves fast in the NE direction. Xinjiang is subject to the northward force imposed by Qinghai-Tibet tectonic block, so the maximum principal compressive stress is mostly in the SN direction. Qinghai-Tibet Plateau is subject to the collision imposed by the Indian Plate, so the maximum principal compressive stress direction is very complex, where it is in NNE direction in the main part and in NNE-NE, NEE, nearly EW, SE and SSE directions along the northern margin extending from southeast to southeast borders. As clearly indicated in Fig. 5, the areas around Qinghai-Tibet Plateau move fast; the northward movement velocity of the tectonic blocks reduces gradually from west to east and they generally revolve clockwise around the Himalaya Mountains; the movement is in NE direction to the east of Qinghai-Tibet Plateau.

The stress between Indian Plate and Eurasian Plate is mostly in EN direction and is largely perpendicular to the plate boundary, which is confirmed by Fig. 5. The great stress values mostly exist on the tectonic boundary between the plates. The maximum value calculated in this paper is > 40 Mpa, which exists on the tectonic boundary. However, they mostly do not coincide with the plate tectonic boundary and their maximum value coincides with the part of the crust with the maximum thickness (Tenzer et al. 2017). Overall, the tectonic stress in China mainland and surrounding regions is very complex, GNSS horizontal velocity field and stress field generally have the same trend and the tectonic stress generally indicates the relevant geological activities.

Fig.4 Tectonic stress field vector in China and surrounding regions
Black solid lines are the state boundaries, where the thick black solid line represents the national boundary of China, the light black solid line represents the boundary of China's provinces, and black arrows denote vectors of the maximum principal compressive stress.

Fig.5 Horizontal GPS velocities in China and surrounding regions (Zhao et al. 2015)

3.3 Boundary identification

On the basis of the Bouguer gravity anomaly data, we calculate the satellite gravity full-tensor gradient data and use the boundary identification methods with various combinations to identify the tectonic boundaries of China and surrounding regions (see Fig. 6 and 7). As indicated in Fig. 6 and 7, in the boundary identification methods, the various components of gravity gradient tensor have different anomaly characteristics, which indicates the boundaries and fracture structures of the geological bodies in the study area: V_{xx} and V_{xz} represent SN anomaly distribution, V_{yy} and V_{yz} represent EW anomaly distribution, V_{xy} represents NE and NW anomaly distribution; V_{zz}, similar to gravity anomaly effect, represents the change rate of gravity anomaly along the vertical direction and reveals more tectonic details. Total horizontal derivative, analytic signal and total horizontal derivative of tilt derivative are obviously advantageous in identifying wide and large fault zones and microplate outlines; Tilt derivative and Theta map are developed from total horizontal derivative and analytic signal and are both angular boundary identification methods, which increase image interpretation resolution and are highly effective in identifying small fractures. Overall, every boundary identification method is limited to various extents in the study area, therefore boundary identification and analysis comprehensively take into account gravity full-tensor gradient and its various combinations, to identify and analyze the tectonic boundaries of East Asia.

Geological data, gravity anomaly, satellite gravity full-tensor gradient and other boundary identification methods are used for boundary identification in East Asia, as shown in Fig. 8. As indicated in Fig. 8, the main fractures identified in this paper are largely consistent with the ones previously identified by other people (Zhang et al. 2013). China is located in the southeast of the

Eurasian Plate and is subject to the effects of subducting, squeezing and collision by the Indian Plate, Philippine Plate and Pacific Plate. As seen in Fig. 8, due to the collision to East Asia caused by the Indian Plate to the southwest, the Himalaya active tectonic belt PB1 becomes the boundary active tectonic belt between Indian Plate and East Asia; The Philippine Plate constantly squeezes the Eurasian Plate in the NW direction and the Taiwan active tectonic belt PB2 becomes the boundary active tectonic belt between these two plates; Northeast China is located in the westmost part of the West Pacific subduction zone (Zhao et al. 2012). According to its gravity anomaly and Fig. 6 and 7, there is an obvious boundary active tectonic belt PB3 between Northeast China, West Pacific and North America Plate. As seen in Fig. 8, No. 3 represents the Zhangjiakou-Bohai fault zone, No. 4 represents the Xinyang-Jinzhai fault zone and the east part of Changhua-Putuo fault zone, No. 5 represents the Red River fault zone, No. 6 represents the Xiaojiang fault zone, No. 7 represents the Longmenshan fault zone, No. 9 represents the Main Himalayan Thrust, No. 14 represents the Haiyuan fault zone and No. 15 represents the Altyn Tagh fault zone; Fig. 2, 6 and 7 clearly indicate the Ordos tectonic block. These contact zones constitute the boundary between the primary tectonic blocks in China and surrounding regions. In Fig. 8, No. 1 represents the TanLu fault zone, No. 2 represents the Shanxi fault zone, No. 10 represents the Jiali fault zone, No. 11 represents the Xianshuihe fault zone, No. 12 represents the Kunlun fault zone, No. 13 represents the West Qinling fault zone, No. 17 and 18 represents the Southern Tianshan and Northern Tianshan fault zones, where the NE extension of TanLu fault zone is the Yilan-Yitong fault zone. These fault zones constitute the boundaries of some of the secondary active tectonic blocks.

It is worth noting that Zhang et al. (2003) deduced that the hidden fault in front of Dabie Mountains was the south boundary of North China Plain tectonic block. This paper believes that

the Xinyang-Jinzhai fault zone and the east part of Changhua-Putuo fault zone may constitute the tectonic unit boundary between North China and South China active tectonic blocks. As seen in Fig. 2, positive and negative values alternate with each other to the north and south of this fault zone, but the south segment has great difference between positive and negative values while the north segment has mild variation; in Fig. 3, the south segment has noticeable difference while the north segment has no noticeable variation; as seen in Fig. 6, the two ends have significant variation in gradient, with the aforesaid fault zone as the boundary; the gradient directions on both sides also have difference; in Fig. 7, the two ends of the fault zone have obviously different colors, which is particularly clear in Fig. 7(a)-7(c). Therefore this paper deduces that Xinyang-Jinzhai fault zone and the east part of Changhua-Putuo fault zone constitute the tectonic unit boundary between the North China and South China active tectonic block regions. As clearly indicated in Fig. 7(d), the Red River fault zone starts from the northwest corner of the South China Sea, extends along a SE anomaly belt, reaches near the Hainan Island, then extends nearly southward and finally connects the Yuedong-Wanan fault zone; In Fig. 7(c) and 7(e), this anomaly belt has obviously different colors than the areas to its sides and there is a noticeable boundary In Fig. 2 and 3, the gravity anomaly value of this anomaly belt is greater than that of the areas to its sides and has great difference from the nearby amplitude; In Fig. 6, both sides of this anomaly belt have significant variation, where the values are greater than or less than this fault zone, with noticeable difference in color. This fact is highly similar to the study result of Dai et al. (2018), therefore this paper believes that the aforesaid anomaly belt is an extension of the Red River fault zone.

3.4 Tectonic zoning

In addition to the above study results, we completed tectonic zoning of China and

surrounding regions by using the boundary identification methods based on the satellite gravity full-tensor gradient data and its combinations and taking into account the zoning principle for the active tectonic blocks of China and surrounding regions proposed by Zhang et al. (2003), the zoning principle for active fault blocks of China mainland proposed by Deng et al. (2003) and the boundary distribution principle for the active tectonic blocks of China mainland proposed by Zhang et al. (2005). This paper identifies in China and surrounding regions 6 primary active tectonic blocks, 22 secondary active tectonic blocks, 3 tertiary active tectonic blocks and 20 active tectonic block boundary zone constituted of deformation belts and active tectonic belts with various geometric structures and width variations. The fault zones analyzed in the previous section are the boundaries of the vast majority of the active tectonic blocks; the secondary fault zones mostly exist in the aforementioned tectonic zones. The grey lines segments in Fig. 8 and Fig. 9 represent the faults in China (from Deng et al. 2003). The following section will describe in detail the aforementioned tectonic zoning results.

Northeast Asia active tectonic block region

Northeast China is located the most active subduction zone in the world, i.e. the westmost part of the West Pacific subduction zone, where it is tectonically stable (Zhao et al. 2012). The prior section identified boundary active tectonic belt P3 between the plates. Fig. 9 shows this region consists of 3 tectonic blocks, i.e. Yanshan, Xing'an-Dongmeng and Dongbei. However, unlike the boundary deduced by Zhang et al. (2003), for the tectonic boundaries identified in Fig. 2, 3, 6 and 7 in this paper, the boundary of the primary active tectonic block regions is adjusted as shown in Fig. 9. The deduced boundary zone has clearly different color and difference value than the surrounding areas and can be clearly distinguished.

North China active tectonic block region

North China active tectonic block region is located to the south of Northeast Asia active tectonic block region. Fig. 9 shows the North China active tectonic block region consists of 3 tectonic blocks, i.e. Ordos, North China Plain and Ludong-Huanghai. Fig. 2, 3, 6 and 7 can all identify the Ordos tectonic block as a tectonic unit. Ordos tectonic block is subject to strong effect of squeezing by the extension of the North China Basin and the northeast margin of Qinghai-Tibet Plateau and is divided by the Shanxi graben basin. This tectonic block is surrounded by very strong tectonic activities; tectonic deformation is dominated by strike-slip movement; it has weak interior tectonic activities; the boundary between the plate and the surrounding geological units is a fault zone. The North China Plain tectonic block has Zhangjiakou-Bohai fault zone as its north boundary, Tan-Lu fault zone as its east boundary, Shanxi graben basin as its west boundary and Xinyang-Jinzhai fault zone and the east part of Changhua-Putuo fault zone as its south boundary, which is also the tectonic unit boundary between the North China and South China active tectonic block regions, as described in detail in the preceding section. Taking into account the zoning principle for North China active tectonic block proposed by Hang et al. (2003) and the internal outlines of North China Plain tectonic block as identified in Fig. 2, 6 and 7, the North China Plain is divided into T'ai-hang tectonic, Jilu and Yuhuai tectonic blocks. While the naming proposed by Han Zhujun et al. is still used, the boundary line is somewhat different. The Z18 and Z19 in Fig. 9 are different from the Tangshan-Hejian-Cixian active tectonic belt identified by Han Zhujun et al. The southwest part of this tectonic belt does not extend in the direction identified previously, but extend towards the fault zone in front of T'ai-hang Mountains.

South China active tectonic block region

South China active tectonic block region is located in Southeast China, in a stable plate, where it is relatively stable geologically. The boundary between this region and North China active tectonic block region is briefly described above. Fig. 9 shows this tectonic block region consists of Huanan and Nanhai tectonic blocks. Unlike the zoning proposed by Zhang et al. (2003), this paper updates zoning of Nanhai tectonic block according to Fig. 2, 3, 6 and 7. The outline of Nanhai tectonic block as show in these figures has drastic variation compared with the surrounding areas, where the anomaly value is greater than or less that of the surrounding areas and there is a clearly visible boundary between the geological tectonic units. Due to length limit of this paper, the boundary of Nanhai tectonic block is not described in detail.

Yunnan-Myanmar active tectonic block region

Yunnan-Myanmar active tectonic block is located in South China, to the south of the east tectonic line of Qinghai-Tibet Plateau. Fig. 9 shows this tectonic block region consists of Western Yunnan and Southern Yunnan tectonic blocks. This tectonic block is dominated by strike-slip earthquake, with complex fault types. Yunnan-Myanmar active tectonic block region is closely adjacent to South China active tectonic block region. Its east boundary is the west margin of South China active tectonic block region and west boundary is the Myanmar arcuate plate subduction zone; in its middle is the Nujiang-Lancangjiang fault zone, which divides this region into Western Yunnan and Southern Yunnan tectonic blocks. Due to scarcity of geophysical data of this region, Fig. 2, 3, 6 and 7 cannot clearly delimit the boundaries of the microplates, therefore Fig. 9 does not completely indicate the detail outline of this region, which entails further study in the future.

Qinghai-Tibet active tectonic block region

Qinghai-Tibet Plateau is a unique geological unit which has complex topography and very

active geological tectonic movement. As seen in Fig. 9, the Qinghai-Tibet Plateau tectonic block has the Altyn Tagh-Haiyuan fault zone as its north boundary, Longmenshan Mountains-Xiaojiang fault zone as its east boundary, Himalaya collision zone as its south boundary and Karakoram fault zone as its west boundary, which is largely identical to the zoning proposed by Tang (2003). Slightly unlike the work of Zhang et al. (2003), this paper identifies West Qinling fault zone, Kunlun fault zone, Xianshuihe fault zone and Jiali fault zone as the boundaries of Qi-lian, Qaidam, Bayan Har, Qiangtang and Lhasa tectonic blocks respectively; the upward extension of Nujiang-Lancangjiang fault zone is the boundary between Yunnan-Myanmar and Qiangtang tectonic blocks. Fig. 9 clearly identifies the boundary of geological units of Qinghai-Tibet active tectonic block region. This region is roughly shaped like a spindle, in which the interior has mild variation while the periphery has drastic variation in amplitude. This active tectonic block region has extensive presence of large number of active faults; the low-altitude areas around the plateau mostly have thrust faults; the interior high-altitude areas are dominated by SN normal faults and conjugated strike-slip faults, which is closely associated with the outward squeezing effect of this tectonic block and the nearly EW extension effect of its interior. The Longmenshan fault zone, Altyn Tagh-Haiyuan fault zone and Himalaya thrust-napped zone are all thrust faults; the East Kunlun fault zone, Xianshuihe fault zone and Jiali fault zone are strike-slip faults.

Since the Cenozoic, the collision and squeezing between the Indian Plate and Eurasian Plate have given rise to the upheaval of the Himalaya Mountains to the south of Yarlung Zangbo River fault. As seen in Fig. 9, the Himalaya active tectonic belt PB1 is located between the Indian Plate and Eurasian Plate, with noticeable anomalies on its both sides. This figure shows anomaly in NW direction. The Altyn Tagh fault zone dominates the north boundary of Qinghai-Tibet Plateau and

plays a crucial role in the process of collision between the Indian Plate and Eurasian Plate. The Altyn Tagh fault zone is in NE direction, with noticeable anomalies on its both sides, and is a recognized boundary. As clearly seen in Fig. 6 and 7, Longmenshan Mountains fault zone is located at the east margin of Qinghai-Tibet Plateau and extends in NW-SE direction; As seen in Fig. 6, Longmenshan Mountains fault zone is located in an obvious transitional zone, with noticeable gradient variation on its both sides, and has very complex geological structure. Qaidam Basin, the largest intermountain sedimentary basin, is located in the northeast of Qinghai-Tibet Plateau, and between its periphery and the neighboring tectonic units are deep large faults, which are mostly thrust-nappe faults and strike-slip faults. As seen in Fig. 6 and 7, the periphery of this basin has drastic variation as compared with the interior blocky areas and has significantly greater value, which perfectly matches the direction of the surrounding fault zones. In Fig. 7, the East Kunlun fault zone is located in the south of Qaidam tectonic block and extends in NWW direction; with the East Kunlun fault zone as the boundary, the upper and lower parts have drastic variation between them, with significantly greater value at the boundary, which is a recognized fault zone.

Western Regions active tectonic block region

The Western Regions tectonic block region is located to the north of Qinghai-Tibet active tectonic block region. Fig. 9, roughly referencing the zoning principle proposed by Zhang et al. (2003) and the zones identified in Fig. 2, 3, 6 and 7, divides this tectonic block into 6 tectonic blocks, i.e. Tarim, Tianshan, Junggar, Alxa, Altai and Sayan. Similar to Northeast Asia active tectonic block region, the outline of this active tectonic block region has been updated according to the identification results in this paper.

Tarim Basin is a stable region in the center of the Tarim plate and is surrounded by the

472 orogenic belts such as Southern Tianshan, West Kunlun and Altyn Tagh. As seen in Fig. 7(c), 7(d)
473 and 7(e), this basin contains a large EW fault zone. As clearly seen in Fig. 6 and 7, the interior of
474 this basin has mild variation as compared with its periphery; the periphery, with drastic amplitude
475 variation, distinguishes the Tarim tectonic block and the surrounding tectonic blocks; the south
476 and north boundaries perfectly match the Southern Tianshan and Altyn Tagh fault zones. Tarim
477 tectonic block is generally a relatively stable tectonic block, but the plate has complex interior
478 structure which is affected by the activities of the peripheral orogenic belts and its boundary is
479 mostly dominated by large fault zones. Tianshan Mountains is located in the north of Tarim
480 tectonic block and south of Junggar tectonic block, it has complex interior structure, deformation
481 mostly occurs in front of and inside mountains and is dominated by foreland basin folds and thrust
482 faults and its periphery is dominated by thrust fault zones. As seen in Fig. 6 and 7, the plate
483 periphery has drastic variation and the Northern Tianshan fault zone in the north and Southern
484 Tianshan in the south clearly distinguish this plate from the surrounding plates. The gradient and
485 fault zone of Tianshan Plate generally extend in EW direction, but its west segment has noticeable
486 anomaly and the fault zone there extends in NNW direction. Junggar tectonic block, located to the
487 north of the Tianshan block, is generally similar to Tarim tectonic block. Its interior has mild
488 variation and the periphery has drastic increase in amplitude.
489
490 Fig.6 Gravity anomaly gradient tensor- $V_{xx}, V_{xy}, V_{xz}, V_{yy}, V_{yz}, V_{zz}$ (a-f)
491
492 Fig.7 Edge Detection data in China and surrounding regions
493 (a) THD; (b) ASM; (c) THDR; (d) TDR; (e) θ
494
495 Fig.8 The main edge results in China and surrounding regions
496 Line 1 is Tanlu fault zone; Line 2 is Shanxi fault zone; Line 3 is Zhangjiakou-Bohai fault zone;

Line 4 is Xinyang-Jinzhai fault and the eastern part of Chang hua-Putuo fault; Line 5 is Red River fault; Line 6 is Xiaojiang fault zone; Line 7 is Longmenshan fault zone; Line 8 is Nujiang-Lancangjiang fault zone; Line 9 is Main Himalayan Thrust; Line 10 is Jiali fault zone; Line 11 is Xianshuihe fault zone; Line 12 is Kunlun fault zone; Line 13 is the West Qinling fault zone; Line 14 is Haiyuan fault zone; Line 15 is Altyn Tagh fault zone; Line 16 is Karakoram zone; Line 17 is Southern Tianshan fault zone; Line 18 is Northern Tianshan fault zone; PB1, PB2, PB3 represents active boundary zone between plates; The purple dotted line indicates the inferred extension of the Red River fault. And the gray solid line indicates other faults. (Deng et al. 2003).

Fig.9 Tectonic division in China and surrounding regions

A is Qinghai-Tibet active tectonic block regions, A1 is Lhasa block, A2 is Qiangtang block, A3 is Yunnan-Sichuan block, A4 is Bayan Har block, A5 is Qaidam block, A6 is Qilian block; B is Western Regions active tectonic block regions, B1 is Tarim block, B2 is Tianshan block, B3 is Junggar block, B4 is Sayan block, B5 is Altai block, B6 is Alxa block; C is Northeast Asia active tectonic block regions, C1 is Xing'an-Dongmeng block, C2 is Yanshanian block, C3 is Northeast block; D is North China active tectonic block regions, D1 is Ordos block, D2 is North China Plain block, D3 is Ludong-Huanghai block, D2-1 is Taihang Mountain block, D2-2 is Ji-Lu block, D2-3 is Yu-Huai block; E is South China active tectonic block regions, E1 is South China block, E2 is South China Sea block; F is Yunnan-Myanmar active tectonic block regions, F1 is Western Yunnan block, F2 is South Yunnan block. P1 is Indian Plate, P2 is Pacific plate, P3 is Philippine Plate, P4 is North America plate. The red solid lines represent the plate active boundary, the blue solid lines represent the first-order active tectonic block boundary, the blue dotted lines indicate the inferred active tectonic block boundary, the green solid lines indicate the second-order active tectonic block boundary, and the yellow solid lines indicate the third-order active block boundary. And the gray solid line indicates other faults. (Deng et al. 2003). Z1-Z20 represents the active tectonic zone between active blocks.

4 Conclusion

By using the satellite gravity data that have high precision, high resolution and ample geophysical information, this paper investigates the gravity anomaly and tectonic boundary characteristics of China and surrounding regions. We use free-air gravity anomaly and topography data to calculate the terrestrial-marine Bouguer gravity anomaly of East Asia and analyze the

528 characteristics of the resources and structures inside the crust that deviate from normal density
529 distribution. We use the Bouguer gravity anomaly to identify the tectonic stress field and discuss
530 the distribution characteristics of the tectonic movements of China and surrounding regions and
531 their dynamics. We use satellite gravity full-tensor gradient data and its combinations to identify
532 the tectonic boundaries of underground faults, contact zones and other tectonic units and thereby
533 divide the geological tectonic units of East Asia, identify the general outlines of the microplates
534 and provide the tectonic basis for geological interpretation. Based on the above methods, we draw
535 the following conclusion:

536 (1) Free-air gravity anomalies alternate with each other, which correspond to the positive and
537 negative structures geologically and the geotectonic structure of China. The east and west parts of
538 China mainland, with largely 105° E between them, have significant difference in Bouguer gravity
539 anomaly. Generally, the eastern anomalies are higher than the western ones and northern ones
540 higher than southern ones. Bouguer gravity anomaly has mild variation in East China and
541 generally reduces gradually from east to west, mostly in NNE direction; West China has drastic
542 variation and gravity anomaly reduces gradually in a wave mode from north to south. Bouguer
543 gravity anomaly is well indicative of the basic geotectonic characteristics of China mainland.

544 (2) Due to the strong effects of the surrounding plates, China and surrounding regions have
545 unique lithospheric stress field and clearly distinguishable zones and the stress generally reduces
546 gradually from west to east. The stress is greater in West China than in East China. West China is
547 subject to squeezing in nearly SN-NNE direction and has complex stress field. The maximum
548 principal compressive stress in Xinjiang exists in SN direction and that in Qinghai-Tibet Plateau
549 mostly changes gradually from NNE to SSE; East China is subject to squeezing in NEE-SWW

direction. From the Northeast tectonic block in Northeast China to the South China tectonic block in the southeast, the maximum principal compressive stress direction gradually changes from NE to WE and then to SE; GNSS horizontal velocity field and stress field generally have the same trend, but the stress filed is indicative of more tectonic activities.

(3) By comprehensively referencing the previous studies on China mainland by other people and by using the boundary identification methods based on the satellite gravity full-tensor gradient data and its combinations, we investigate the tectonic boundary characteristics of China and surrounding regions. Section 3.3 updates the extension route of Red River fault zone and speculates that this fault extends in SE direction to the Hainan Island and then extends nearly southward to connect the Yuedong-Wanan fault zone; It is deduced that Xinyang-Jinzhai fault zone and the east part of Changhua-Putuo fault zone may constitute the tectonic unit boundary between the North China and South China active tectonic block regions. Section 3.4 identifies in China and surrounding regions 6 primary active tectonic blocks, 22 secondary active tectonic blocks, 3 tertiary active tectonic blocks and the 20 active tectonic block boundary zones constituted of deformation belts and active tectonic belts with various geometric structures and width variations. The main contact zones are the boundaries of the vast majority of the active tectonic blocks, while the secondary faults are mostly present within the aforesaid tectonic zones.

Abbreviation

SIO: Scripps Institution of Oceanography; THD: total horizontal derivative; ASM: analytic signal; TDR: tilt derivative; THDR: total horizontal derivative of the tilt derivative; EGM2008: Earth Gravitational Model, 2008.

Acknowledgements

We thank the D. Sandwell of UCSD for providing the gravity model and topography model. We also express our sincere gratitude to the editors and reviewers in improving the manuscript. All figures were created using Generic Mapping Tools software (Wessel and Smith 1998).

Authors' contributions

ZX performed all the analysis and wrote the manuscript. DG analyzed the results and supervised all the work. PZ contributed to improving figures and the revision of the manuscript. All authors read and approved the final manuscript.

Funding

This work is supported by the Basic Frontier Science Research Program of Chinese Academy of Sciences (Grant No. ZDBS-LY-DQC028) and Independent project of State Key Laboratory of Geodesy and Earth's Dynamics (Grant No. E025011010).

Availability of data and materials

The gravity model and topography model was obtained at ftp://topex.ucsd.edu/pub/archive/.

Competing interests

The authors declare that they have no competing interests.

References

Chris W, Carlos P, Peter K (2005) Theta map: Edge detection in magnetic data. Society of Exploration Geophysicists 70(4).

590 Cordell L (1979) Gravimetric expression of graben faulting in Santa Fe Country and the Espanola
591 Basin, New Mexico. In: Ingersoll, R. V. (Ed.), Guidebook to Santa Fe Country, 30th Field
592 Conference. New Mexico Geological Society, pp. 59-64.
593 Cordell L, Grauch, VJS (1985) 16. Mapping basement magnetization zones from aeromagnetic
594 data in the San Juan Basin, New Mexico. Utility of Regional Gravity and Magnetic Anomaly
595 Maps 181-197. doi:10.1190/1.0931830346.ch16.
596 Dai WM, Huang DN, Li LT, et al (2018) The edge detection method and its application in the
597 south China sea based on the gravity gradient structure tensor eigenvalue. Chinese J.
598 Geophys 61(6):2494-2507 (in Chinese with English abstract). doi:10.6038/cjg2018M0018.
599 Deng QD, Zhang PZ, Ran YK, Yang XP, Yan W, Chen LC (2003) Active tectonics and earthquake
600 activities in China. Earth Science Frontiers (S1):66-73 (in Chinese with English abstract)
601 Deng QD, Zhang PZ, Ran YK, Yang XP, Yan W, Chu QZ (2002) Basic characteristics of active
602 tectonics in China. Science in China (Series D) 2002(12):1020-1030+1057 (in Chinese)
603 Fullea J, Fernàndez M, Zeyen H (2008) FA2BOUG—A FORTRAN 90 code to compute Bouguer
604 gravity anomalies from gridded free-air anomalies: Application to the Atlantic-Mediterranean
605 transition zone. Computers and Geoences 34(12):1665-1681.
606 Guo FX, Sun ZM, Zhai ZH, Xiao Y (2017) Tectonic stress field in Bohai Bay area inversed by
607 multi-source gravity observation data. Geomatics and Information Science of Wuhan
608 University 42(01):136-142 (in Chinese with English abstract)
609 Han ZJ, Xu J, Ran YK, et al (2003) Activity block and strong earthquake activities in North China.
610 Science in China (Series D) 33(S1):108-118 (in Chinese)
611 Huang JQ, Ren JS, Jiang CF, Zhang ZK, Qin DY (1980) The Geotectonic Evolution of China.

612 Science Press, Beijing (in Chinese)

613 Li CY, Wang Q, Liu XY, et al (1982) Tectonic map of Asia. Cartographic Publishing House,
614 Beijing (in Chinese)

615 Li SG (1973) Introduction to Geomechanices. Science Press, Beijing (in Chinese)

616 Lu ZZ, Li CF, Zhu S, Audet Pascal (2020) Effective elastic thickness over the Chinese mainland
617 and surroundings estimated from a joint inversion of Bouguer admittance and coherence.
618 Elsevier (prepublish)

619 Ma ZJ, Gao XL, Song ZF (2006) Analysis and tectonic interpretation to the horizontal
620 gradientmap calculated from Bouguer gravity data in the China mainland. Chinese J.
621 Geophys, 49(1):106-114 (in Chinese with English abstract)

622 Mickus KL, Hinojosa JH (2001) The complete gravity gradient tensor derived from the vertical
623 component of gravity: a Fourier transform technique. Journal of Applied Geophysics
624 46(3):159-174.

625 Miller HG, Singh V (1994) Potential field tilt—a new concept for location of potential field
626 sources. Journal of Applied Geophysics 32(2-3):213-217.

627 Nabighian, Misac N (1984) Toward a three-dimensional automatic interpretation of potential field
628 data via generalized Hilbert transforms: Fundamental relations. Geophysics 49(6):44-48.

629 Pan GT, Xiao QH (2015) Explanatory Note to the Tectonic Map of China (1:2,500,000).
630 Geological Publishing House, Beijing (in Chinese)

631 Pan GT, Xiao QH, Lu SN, Deng JF, Feng YM, Zhang KX, Zhang ZY, Wang FG, Xing GF, Hao GJ,
632 Feng YF (2009) Subdivision of tectonic units in China. Geology in China 36(1):1-28 (in
633 Chinese with English abstract).

634 Ren JS, Wang ZX, Chen BW, et al (1999) The tectonics of China from A Global View-A Guide to
635 the Tectonic Map of China and Adjacent Regions. Geological Publishing House, Beijing (in
636 Chinese)
637 Roest WR (1992) Magnetic interpretation using the 3-D analytic signal. Geophysics
638 57(1):116-125.
639 Tang FT (2003) A study on the characteristics of recent tectonic deformation and earthquake
640 activity in North China. Graduate Institute of Geology, China Earthquake Administration,
641 Beijing (in Chinese with English abstract)
642 Tenzer R, Eshagh M, Shen W (2017) The sub-crustal stress estimation in central Eurasia from
643 gravity, terrain and crustal structure models. Geosciences Journal 21(1):47-54.
644 Verduzco B. et al (2004) New insights into magnetic derivatives for structural mapping. The
645 Leading Edge v. 23, p. 116-119.
646 Wei MH, Wang QM, Shi ZH, Yin XH, Liu ZO, Zhang YM (1981) A preliminary study of the free
647 air gravity field in China continent. Seismology and Geology (03):47-60 (in Chinese with
648 English abstract)
649 Wessel P, Smith WHF (1998) New, improved version of the Generic Mapping Tools released. EOS
650 Trans Am Geophys Union 79(47):579.
651 Xie FR, Cui XF, Zhao JT, et al (2004) Regional division of the recent tectonic stress field in China
652 and adjacent areas. Chinese J. Geophys 47(4):654-662 (in Chinese with English abstract)
653 Xiong SQ, Ding YY, Li ZK (2015a) Map of Magnetic Basement Depth in Chinese Continent
654 (1:2,500,000). Geological Publishing House, Beijing (in Chinese)
655 Xiong SQ, Ding YY, Li ZK (2015b) Map of Regional Structure in Chinese Continent

(1:2,500,000). Geological Publishing House, Beijing (in Chinese)

Xiong SQ, Fan ZG, Zhang HR (2015c) Series Map of Aeromagnetic in Chinese Continent and Its Explanatory Note (1:2,500,000). Geological Publishing House, Beijing (in Chinese)

Xiong SQ, Yang H, Ding YY, Li ZK (2018) Subdivision of tectonic units in China based on aeromagnetic data. Geology in China 45(4):658-680 (in Chinese with English abstract)

Xu JR, Zhao ZX, Ishikawa Yuzo (2008) Regional characteristics of crustal stress field and tectonic motions in and around Chinese mainland. Chinese J. Geophys 51(3):770-781 (in Chinese with English abstract)

Yang WC, Chen ZX, Hou ZZ, Meng XH (2016) Crustal density structures around Chinese continent by inversion of satellite gravity data. Acta Geologica Sinica, 90(09):2167-2175 (in Chinese with English abstract)

You YX (1994) A Research on the Conversion of Gravity Field into Regional Tectonic Stress Field. Acta Geophysica Sinica, 37(s):259-272 (in Chinese with English abstract)

Zhang GM, Ma HS, Wang H, et al (2005) Boundaries between active tectonic blocks and strong earthquakes in the China mainland. Chinese J. Geophys (in Chinese with English abstract), 48(3):602-610.

Zhang PZ, Deng QD, Zhang GM, et al (2003) Strong earthquake activities and activities in mainland China. Science in China (Series D) 33(S1):12-20 (in Chinese)

Zhang PZ, Deng QD, Zhang ZQ, et al (2013) Active faults, earthquake hazards and associated geodynamic processes in continental China. Scientia Sinica Terrae 43:1607-1620 (in Chinese)

Zhang WY (1986) Tectonics of Land and Sea in China and Its Adjacent Area. Science Press

678 Beijing (in Chinese)

679 Zhao B, Huang Y, Zhang CH, Wang W, Tan K, Du RL (2015) Crustal deformation on the Chinese

680 mainland during 1998—2004 based on GPS data. Geodesy and Geodynamics 6(01):7-15.

681 Zhao ST, Jin ZM, Gan W (2012) A preliminary study of the focal mechanism of the deep-focus

682 earthquakes in Northeast China. Earth Science Frontiers 19(05):300-311 (in Chinese with

683 English abstract)

Figures

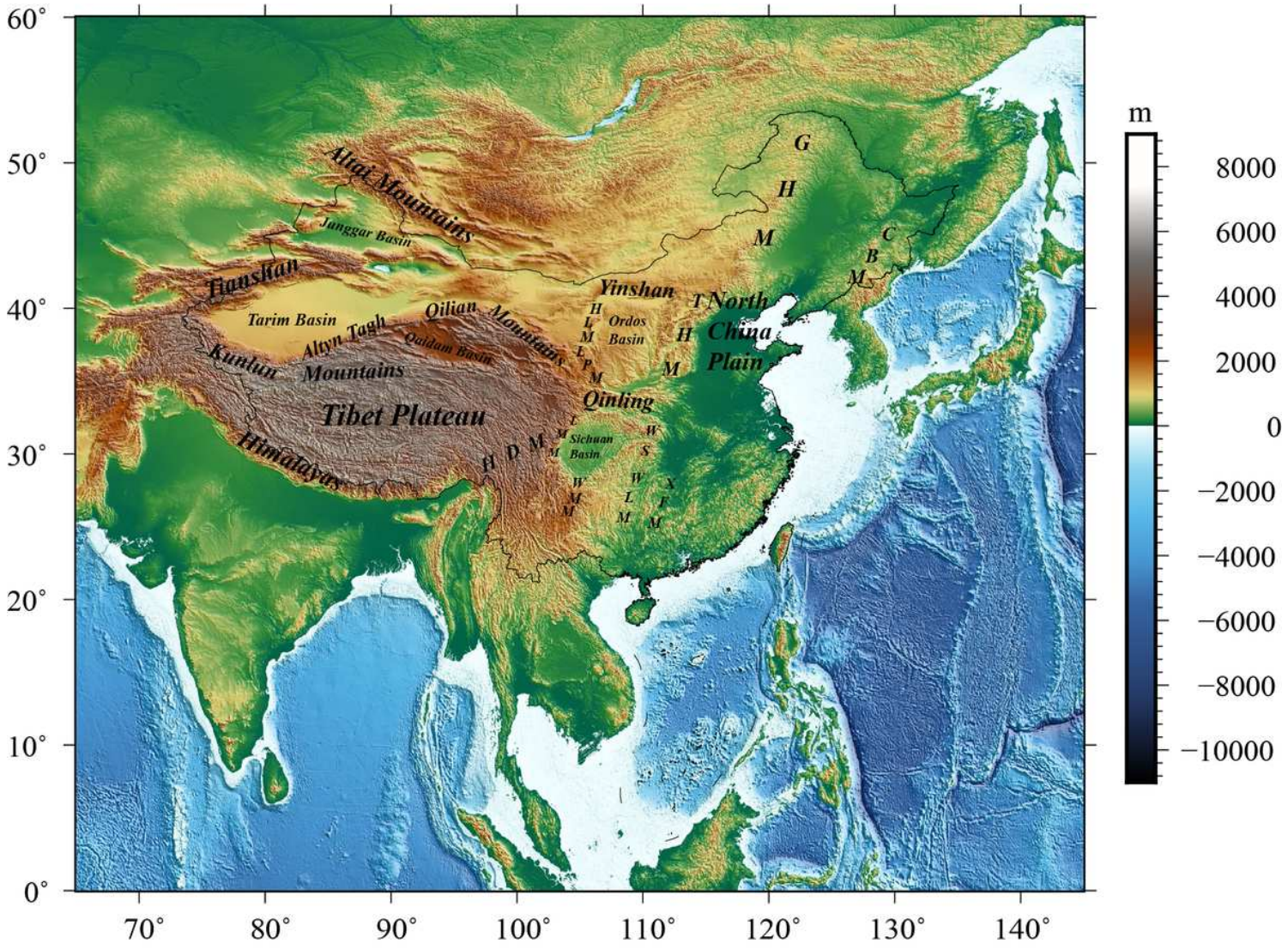

Figure 1

The topographic map in China and surrounding regions Black solid line represents the national boundary of China. HDM (Hengduan Mountains), GHM (Great Higgnan Mountains), CBM (Changbai Mountains), THM (Taihang Mountains), HLM (Helan Mountains), LPM (Liupan Mountains), LMM (Longmenshan Mountains), WS (Wu Shan), WMM (Wumeng Mountains), WLM (Wuling Mountains), XFM (Xuefeng Mountains). The symbols in the following figures have the same meaning. Note: The designations employed and the presentation of the material on this map do not imply the expression of any opinion whatsoever on the part of Research Square concerning the legal status of any country, territory, city or area or of its authorities, or concerning the delimitation of its frontiers or boundaries. This map has been provided by the authors.

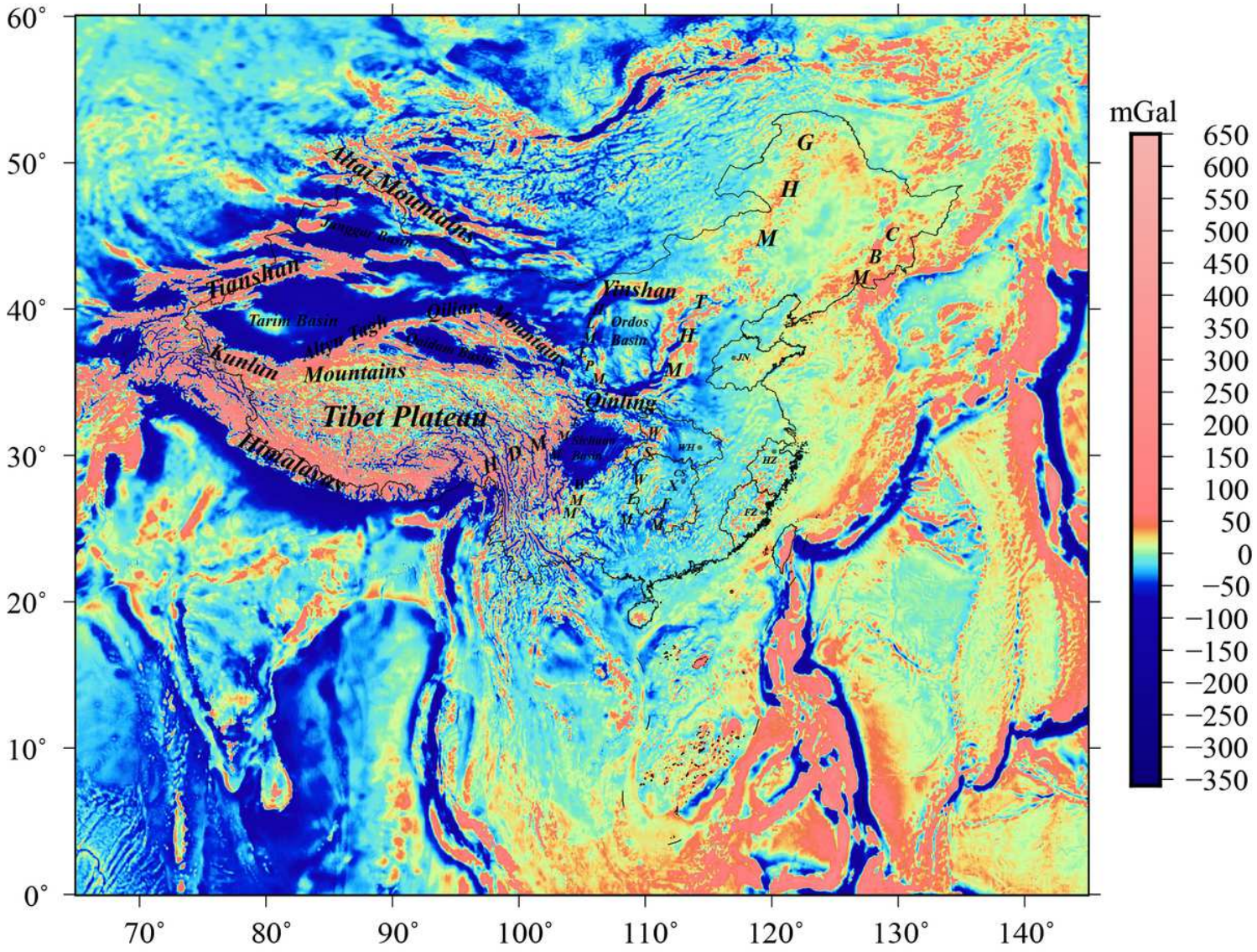

Figure 2

The Free Air gravity anomaly in China and surrounding regions JN is Jinan, the capital of Shandong Province; WH is Wuhan, the capital of Hubei Province; CS is Changsha, the capital of Hunan Province; HZ is Hangzhou, the capital of Zhejiang Province; FZ is the capital of Fujian Province. The symbols in the following figures have the same meaning. Note: The designations employed and the presentation of the material on this map do not imply the expression of any opinion whatsoever on the part of Research Square concerning the legal status of any country, territory, city or area or of its authorities, or concerning the delimitation of its frontiers or boundaries. This map has been provided by the authors.

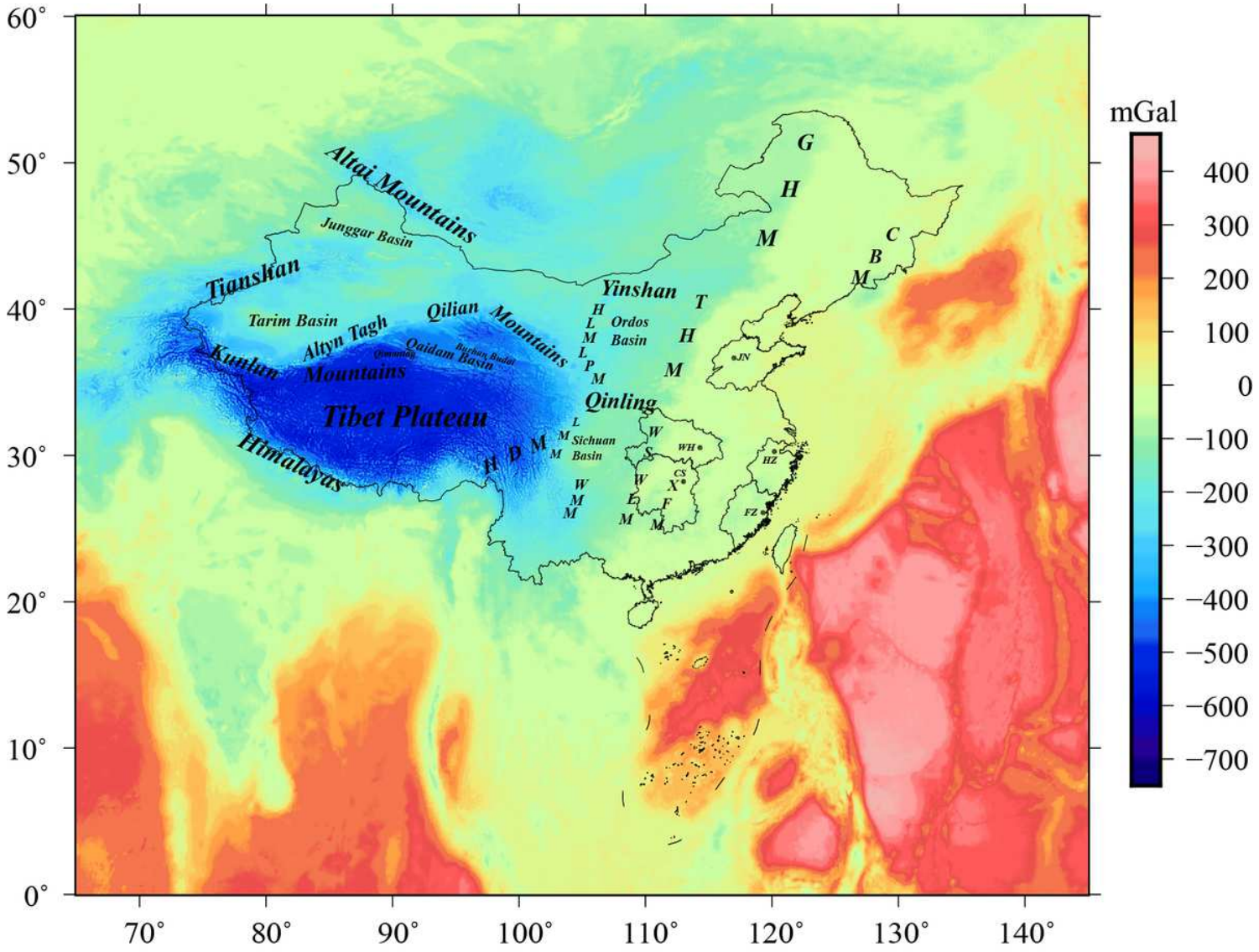

Figure 3

The Bouguer gravity anomaly in China and surrounding regions Note: The designations employed and the presentation of the material on this map do not imply the expression of any opinion whatsoever on the part of Research Square concerning the legal status of any country, territory, city or area or of its authorities, or concerning the delimitation of its frontiers or boundaries. This map has been provided by the authors.

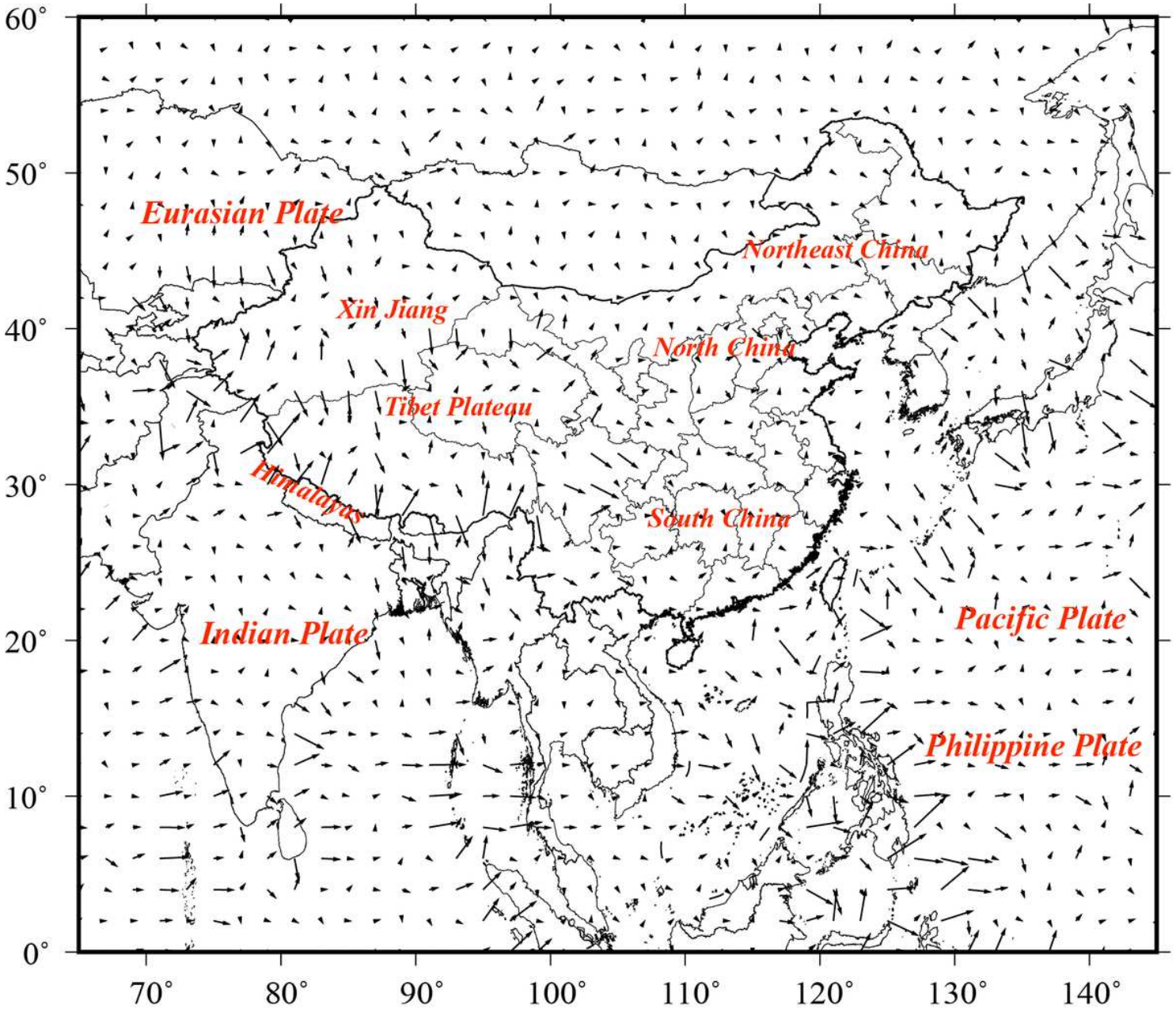

Figure 4

4 Tectonic stress field vector in China and surrounding regions Black solid lines are the state boundaries, where the thick black solid line represents the national boundary of China, the light black solid line represents the boundary of China's provinces, and black arrows denote vectors of the maximum principal compressive stress. Note: The designations employed and the presentation of the material on this map do not imply the expression of any opinion whatsoever on the part of Research Square concerning the legal status of any country, territory, city or area or of its authorities, or concerning the delimitation of its frontiers or boundaries. This map has been provided by the authors.

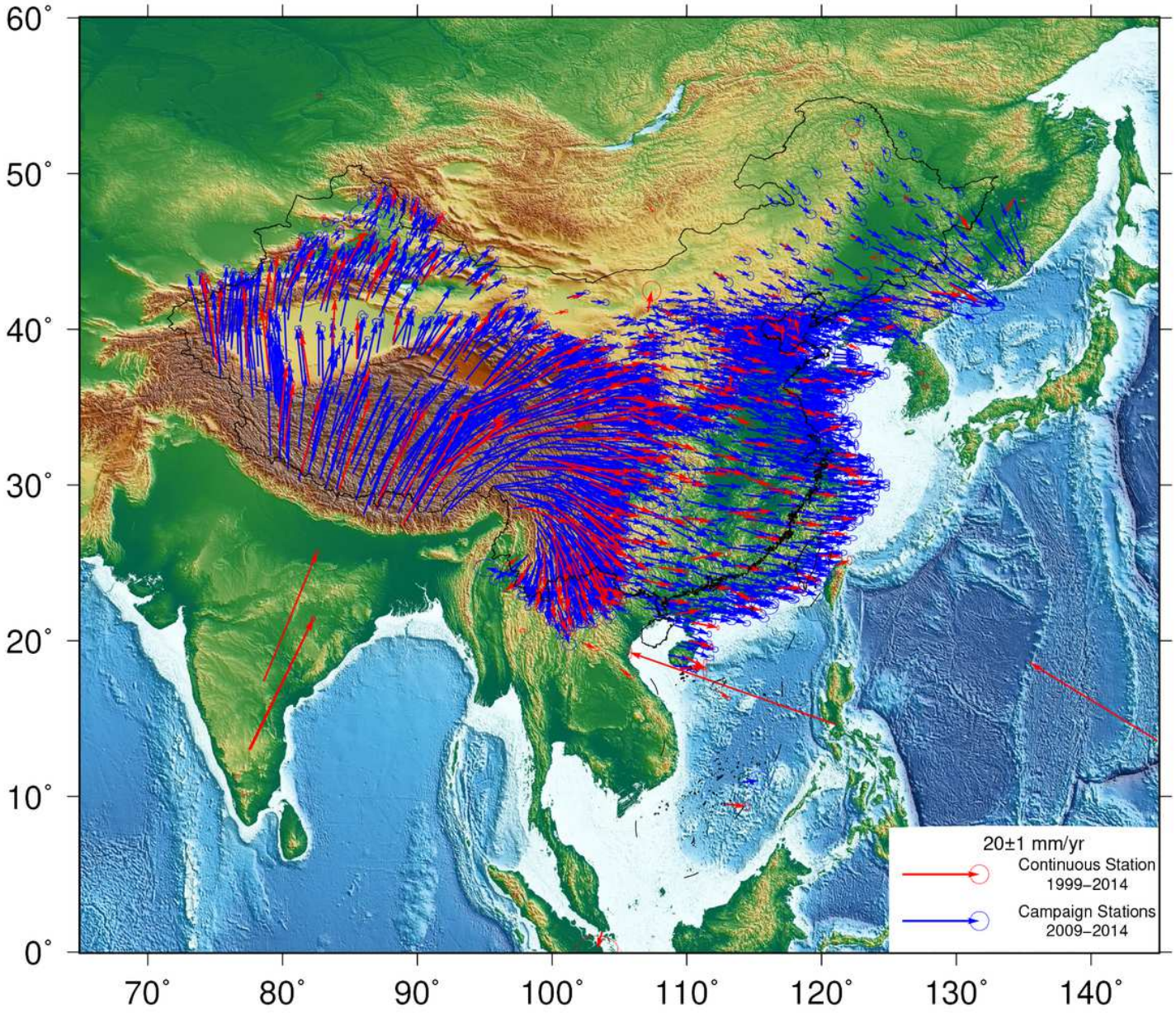

Figure 5

Horizontal GPS velocities in China and surrounding regions (Zhao et al. 2015) Note: The designations employed and the presentation of the material on this map do not imply the expression of any opinion whatsoever on the part of Research Square concerning the legal status of any country, territory, city or area or of its authorities, or concerning the delimitation of its frontiers or boundaries. This map has been provided by the authors.

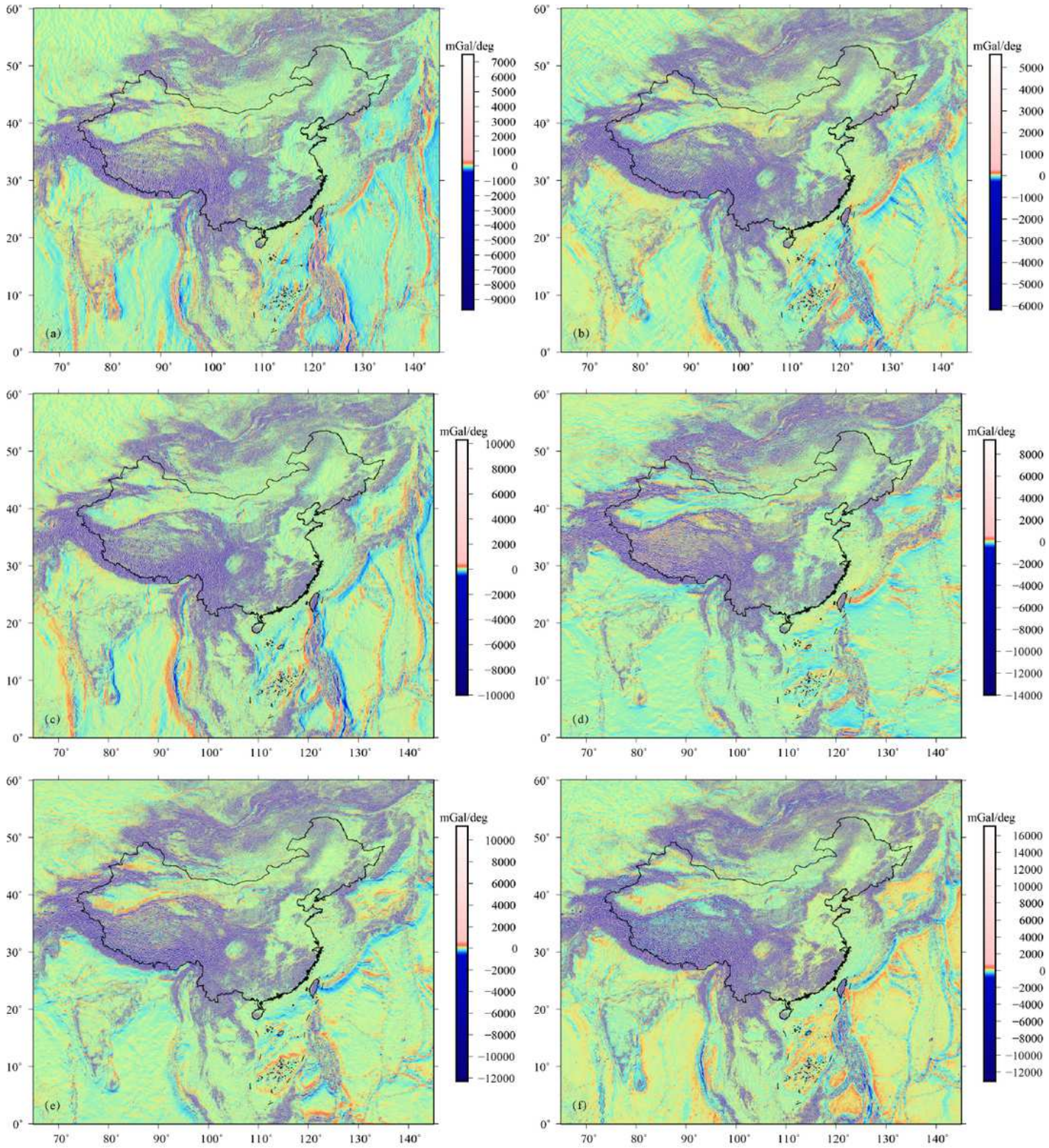

Figure 6

Gravity anomaly gradient tensor- Vxx, Vxy, Vxz, Vyy, Vyz, Vzz (a-f) Note: The designations employed and the presentation of the material on this map do not imply the expression of any opinion whatsoever on the part of Research Square concerning the legal status of any country, territory, city or area or of its authorities, or concerning the delimitation of its frontiers or boundaries. This map has been provided by the authors.

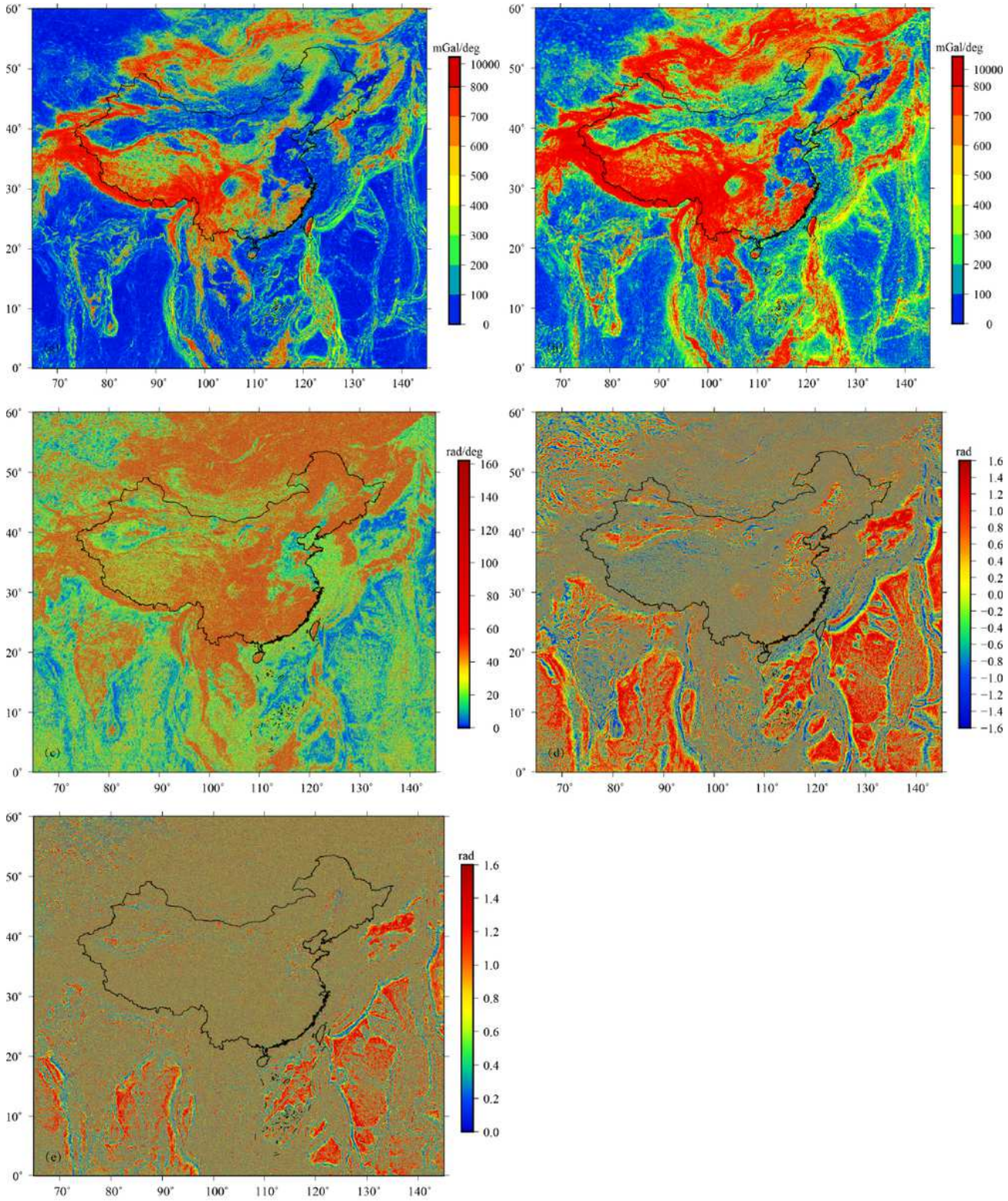

Figure 7

Edge Detection data in China and surrounding regions (a) THD; (b) ASM; (c) THDR; (d) TDR; (e) θ Note: The designations employed and the presentation of the material on this map do not imply the expression of any opinion whatsoever on the part of Research Square concerning the legal status of any country, territory, city or area or of its authorities, or concerning the delimitation of its frontiers or boundaries. This map has been provided by the authors.

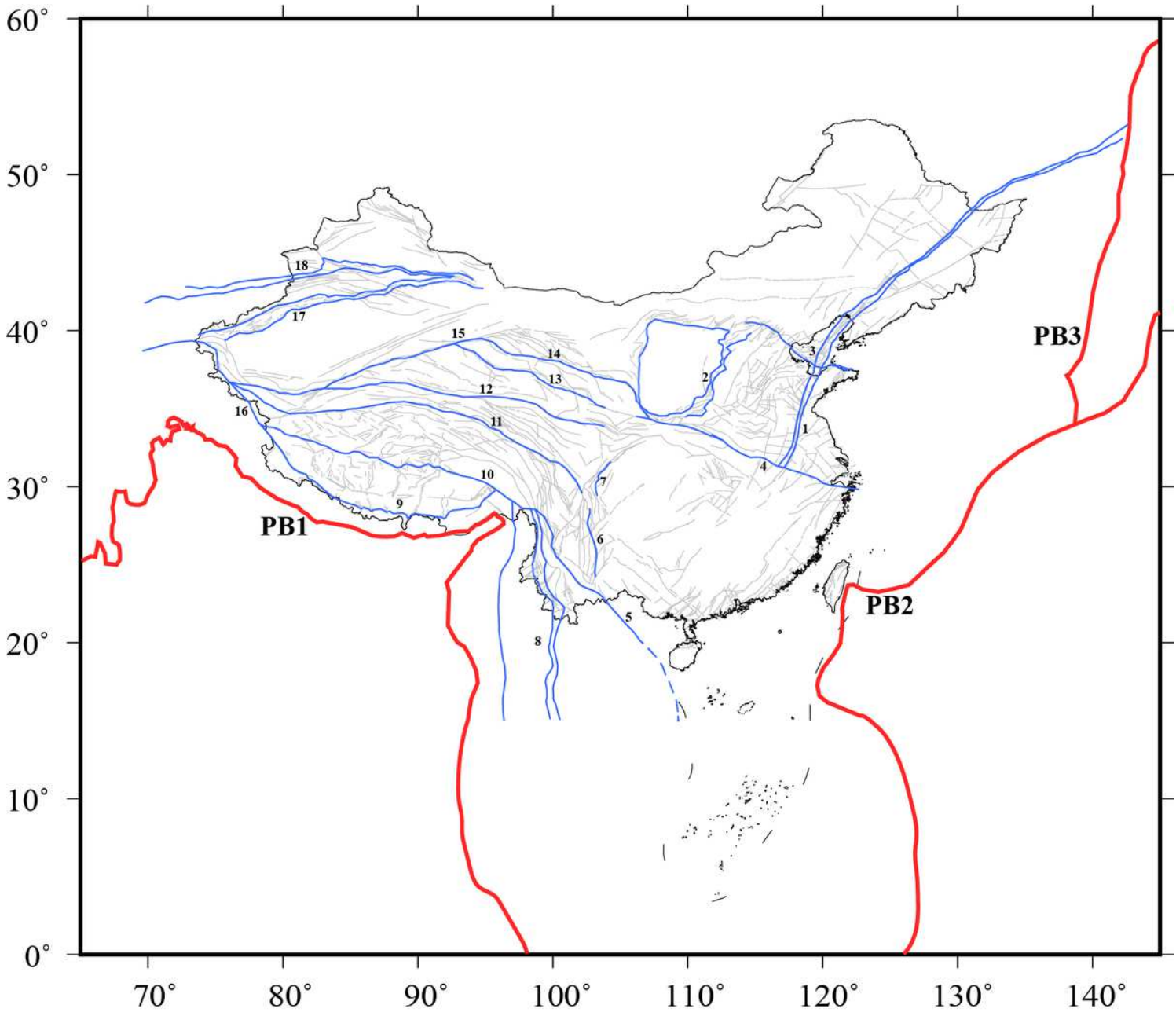

Figure 8

The main edge results in China and surrounding regions Line 1 is Tanlu fault zone; Line 2 is Shanxi fault zone; Line 3 is Zhangjiakou-Bohai fault zone; Line 4 is Xinyang-Jinzhai fault and the eastern part of Chang hua-Putuo fault; Line 5 is Red River fault; Line 6 is Xiaojiang fault zone; Line 7 is Longmenshan fault zone; Line 8 is Nujiang-Lancangjiang fault zone; Line 9 is Main Himalayan Thrust; Line 10 is Jiali fault zone; Line 11 is Xianshuihe fault zone; Line 12 is Kunlun fault zone; Line 13 is the West Qinling fault zone; Line 14 is Haiyuan fault zone; Line 15 is Altyn Tagh fault zone; Line 16 is Karakoram zone; Line 17 is Southern Tianshan fault zone; Line 18 is Northern Tianshan fault zone; PB1, PB2, PB3 represents active boundary zone between plates; The purple dotted line indicates the inferred extension of the Red River fault. And the gray solid line indicates other faults. (Deng et al. 2003). Note: The designations employed and the presentation of the material on this map do not imply the expression of any opinion

whatsoever on the part of Research Square concerning the legal status of any country, territory, city or area or of its authorities, or concerning the delimitation of its frontiers or boundaries. This map has been provided by the authors.

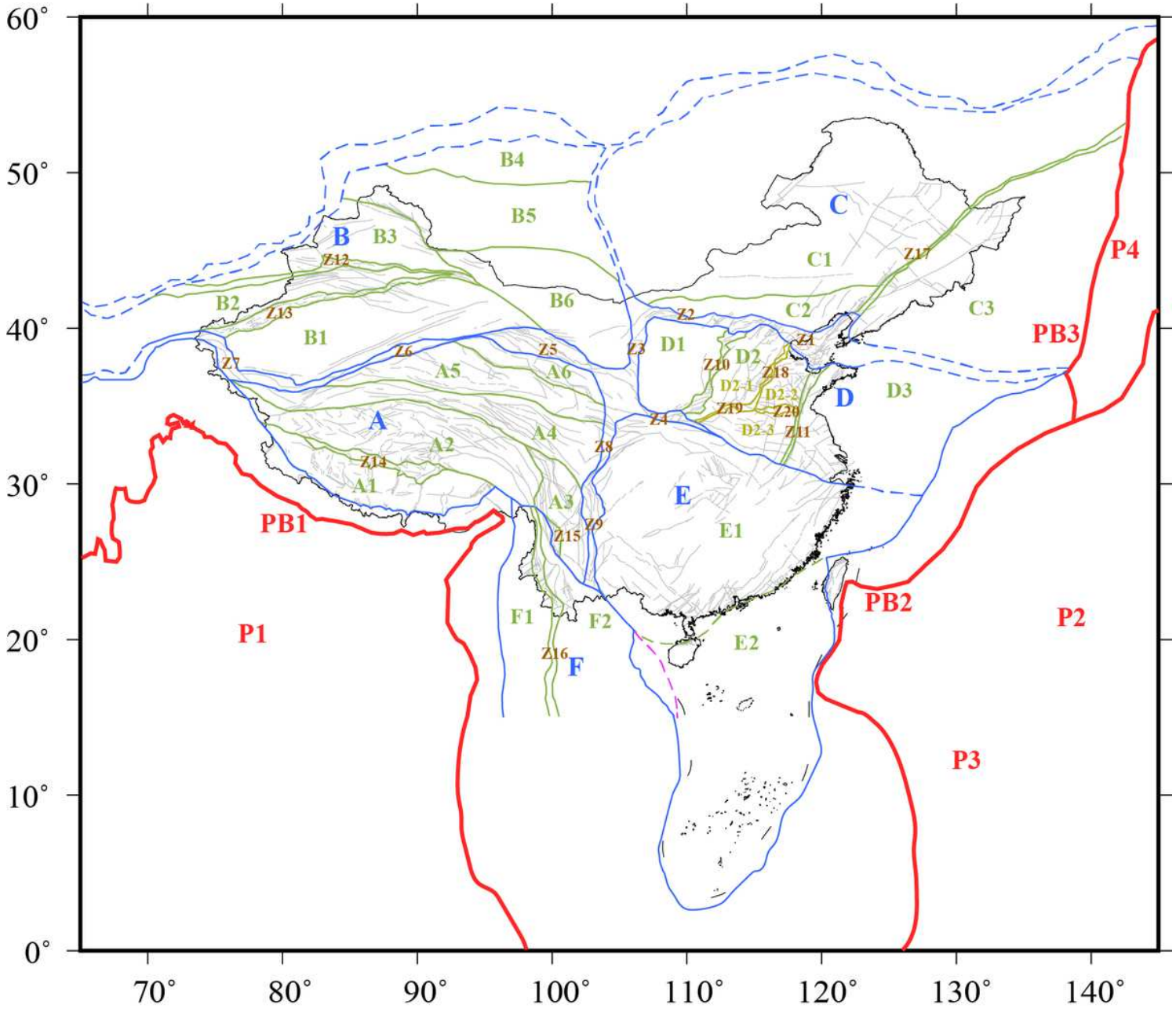

Figure 9

Tectonic division in China and surrounding regions A is Qinghai-Tibet active tectonic block regions, A1 is Lhasa block, A2 is Qiangtang block, A3 is Yunnan-Sichuan block, A4 is Bayan Har block, A5 is Qaidam block, A6 is Qilian block; B is Western Regions active tectonic block regions, B1 is Tarim block, B2 is Tianshan block, B3 is Junggar block, B4 is Sayan block, B5 is Altai block, B6 is Alxa block; C is Northeast Asia active tectonic block regions, C1 is Xing'an-Dongmeng block, C2 is Yanshanian block, C3 is Northeast block; D is North China active tectonic block regions, D1 is Ordos block, D2 is North China Plain block, D3 is Ludong-Huanghai block, D2-1 is Taihang Mountain block, D2-2 is Ji-Lu block, D2-3 is Yu-Huai

block; E is South China active tectonic block regions, E1 is South China block, E2 is South China Sea block; F is Yunnan-Myanmar active tectonic block regions, F1 is Western Yunnan block, F2 is South Yunnan block. P1 is Indian Plate, P2 is Pacific plate, P3 is Philippine Plate, P4 is North America plate. The red solid lines represent the plate active boundary, the blue solid lines represent the first-order active tectonic block boundary, the blue dotted lines indicate the inferred active tectonic block boundary, the green solid lines indicate the second-order active tectonic block boundary, and the yellow solid lines indicate the third-order active block boundary. And the gray solid line indicates other faults. (Deng et al. 2003). Z1-Z20 represents the active tectonic zone between active blocks. Note: The designations employed and the presentation of the material on this map do not imply the expression of any opinion whatsoever on the part of Research Square concerning the legal status of any country, territory, city or area or of its authorities, or concerning the delimitation of its frontiers or boundaries. This map has been provided by the authors.

Supplementary Files

This is a list of supplementary files associated with this preprint. Click to download.

- GraphicalAbstract.png